

Cite this: *RSC Adv.*, 2018, 8, 27073

# Flake-like InVO<sub>4</sub> modified TiO<sub>2</sub> nanofibers with longer carrier lifetimes for visible-light photocatalysts

Yun Zhou,<sup>ab</sup> Lixin Liu,<sup>b</sup> Tao Wu,<sup>b</sup> Guolong Yuan,<sup>a</sup> Junyu Li,<sup>ab</sup> Qiujie Ding,<sup>ab</sup> Fugang Qi,<sup>a</sup> Wenjun Zhu,<sup>b</sup> Xiaoping OuYang<sup>\*a</sup> and Yuan Wang<sup>id</sup><sup>\*b</sup>

Highly efficient solar light absorption capabilities and quantum yields in photocatalysts are key to their application in photocatalytic fields. Towards this end, TiO<sub>2</sub>/InVO<sub>4</sub> nanofibers (NFs) have been designed and fabricated successfully by a one-pot electrospinning process. The resulting TiO<sub>2</sub>/InVO<sub>4</sub> NFs display excellent visible-light photocatalytic activity, owing to their prominent visible-light absorption and electron–hole separation properties. Time-resolved transient PL spectroscopy demonstrated that the TiO<sub>2</sub>/InVO<sub>4</sub> NFs display longer emission decay times (22.0 ns) compared with TiO<sub>2</sub> NFs (15.5 ns), implying that the heterojunction can remarkably suppress the electron–hole recombination and promote the carrier transfer efficiency. With tailored heterostructure features, TiO<sub>2</sub>/InVO<sub>4</sub> NFs exhibit superior visible-light photodegradation activity, and after 80 min of visible-light irradiation, almost 95% of RhB molecules can be decomposed by TiO<sub>2</sub>/InVO<sub>4</sub> NFs, while only 18% of RhB molecules can be decomposed by pure TiO<sub>2</sub> NFs.

Received 22nd May 2018

Accepted 23rd July 2018

DOI: 10.1039/c8ra04344b

rsc.li/rsc-advances

## 1. Introduction

Nowadays, with the overuse of various dyes and plastic products, organic pollutants in water and soil have drawn increasing attention. Among the various strategies, the development of efficient photocatalysts is a promising method for the treatment of organic pollutants, owing to its utilization of abundant solar energy, as well as its low cost and lack of secondary pollution during the course of decomposition.<sup>1–3</sup> Since A. Fujishima discovered the interesting phenomenon of light-induced water splitting by TiO<sub>2</sub> in the 1970s,<sup>4</sup> TiO<sub>2</sub> materials have been the most promising candidates for photocatalytic decontamination on account of their non-toxic, non-luminous corrosion, inert chemical properties, high photocatalytic activity, low cost, and cycle stability.<sup>5–7</sup> However, further application of TiO<sub>2</sub> photocatalysts is unfortunately limited by their large bandgap energy and short photogenerated carrier lifetimes.<sup>8</sup> To overcome these limitations, persistent research, such as non-metal element or metal ion doping,<sup>9–11</sup> surface modification,<sup>12</sup> semiconductor/metal combination,<sup>13,14</sup> and semiconductor/semiconductor hybridization,<sup>15–17</sup> has been engaged in order to narrow the bandgap energy for better visible-light absorption and promote electron–hole separation for longer carrier lifetimes. Herein,

constructing a TiO<sub>2</sub>-based semiconductor/semiconductor nanoheterostructured photocatalyst is an efficient method to increase visible-light harvesting and meanwhile suppress electron–hole recombination, ultimately leading to photocatalytic activity improvement.<sup>18</sup> Up until now, many TiO<sub>2</sub>-based nanoheterostructures with excellent photocatalytic performance have been reported, such as TiO<sub>2</sub>/SnO<sub>2</sub>,<sup>19</sup> TiO<sub>2</sub>/ZnO,<sup>20</sup> TiO<sub>2</sub>/CdS,<sup>21</sup> TiO<sub>2</sub>/MoS<sub>2</sub>,<sup>22</sup> TiO<sub>2</sub>/g-C<sub>3</sub>N<sub>4</sub>,<sup>23</sup> TiO<sub>2</sub>/CuInS<sub>2</sub>,<sup>24</sup> *etc.* Therefore, designing and constructing impactful nanoheterostructures is an effectual way to extend the lifetime of the photogenerated charge, and consequently improve the photocatalytic activity.

InVO<sub>4</sub> semiconductors, as an important group of semiconductors, have attracted much interest because of their potential applications in visible-light-driven photocatalysis, photoelectrochemistry, and gas sensing.<sup>25,26</sup> In particular, InVO<sub>4</sub> is considered to be an ideal choice for coupling with TiO<sub>2</sub> to improve the visible-light photocatalytic performance due to its relatively low bandgap energy ( $E_g \approx 2.1$  eV) and energy level matching with TiO<sub>2</sub>. Up till now, the process for fabricating TiO<sub>2</sub>/InVO<sub>4</sub> NFs usually involves a few synthesis steps, including loading TiO<sub>2</sub> or InVO<sub>4</sub> particles on the surface of InVO<sub>4</sub> or TiO<sub>2</sub>, such as *via* a hydrothermal method followed by an ion impregnate method.<sup>27–29</sup> Hence, the fabrication method for TiO<sub>2</sub>/InVO<sub>4</sub> nanoheterostructures needs to be simplified. Furthermore, although previous research has revealed that TiO<sub>2</sub>/InVO<sub>4</sub> heterostructures exhibit enhanced UV-Vis and visible-light photocatalytic performance, in-depth analysis of the charge transfer and carrier lifetimes of the nanoheterostructure is still missing. For example, Ge *et al.* explored

<sup>a</sup>School of Materials Science and Engineering, Xiangtan University, Xiangtan 411105, Hunan, China. E-mail: oyxp2003@xatu.cn

<sup>b</sup>National Key Laboratory for Shock Wave and Detonation Physics, Institute of Fluid Physics, China Academy of Engineering Physics, P.O. Box 919-111, Mianyang, Sichuan 621900, People's Republic of China. E-mail: wangyuan0000@gmail.com

the visible-light photocatalytic performance of an  $\text{InVO}_4$ - $\text{TiO}_2$  photocatalyst synthesized by a sol-gel method, whereas further discussion on the photocatalytic improvement mechanism is absent.<sup>30</sup> Shen and Perales-Martínez proposed a mechanism for the electron-hole separation process in  $\text{TiO}_2/\text{InVO}_4$  composites only based on the energy band structure, without intuitive experimental characterization.<sup>27,28</sup> Thus, it is necessary to further study the charge transfer and lifetime of the photo-generated charges of  $\text{TiO}_2/\text{InVO}_4$  composites, and it should be clarified as to how much the heterojunction contributes to electron transport, and for how long the carrier lifetime can be obtained through separation at the interface of the heterojunction. Hence, the charge transfer mechanism and carrier lifetime of  $\text{TiO}_2/\text{InVO}_4$  nanoheterostructures need to be analyzed in-depth.

In this paper, we successfully synthesized  $\text{TiO}_2/\text{InVO}_4$  NFs by a one-pot electrospinning method for the first time, which could provide ample heterojunction interfaces as separation channels for photogenerated electron-hole pairs. Moreover, time-resolved transient PL spectroscopy was employed to confirm the carrier lifetime of the  $\text{TiO}_2/\text{InVO}_4$  NFs. With the tailored nanoheterostructures, the prepared  $\text{TiO}_2/\text{InVO}_4$  NFs exhibited enhanced photocatalytic activity due to broadened visible-light harvesting and efficiently prolonged carrier lifetimes resulting from the nanoheterojunction formed between  $\text{TiO}_2$  and  $\text{InVO}_4$ .

## 2. Materials and methods

### 2.1 Synthesis of $\text{TiO}_2/\text{InVO}_4$ NFs

$\text{TiO}_2/\text{InVO}_4$  NFs were synthesized by a one-pot electrospinning process, as shown in Fig. 1(a). Briefly, 0.19 g  $\text{In}(\text{NO}_3)_3 \cdot 4.5\text{H}_2\text{O}$ , 0.18 g  $\text{VO}(\text{acac})_2$ , 0.68 g tetrabutyl titanate (TBT), and 0.4 g polyvinylpyrrolidone (PVP) were added into a mixed solution of 2 g dimethylacetamide (DMAC), 1.0 ml ethanol, and 0.8 ml acetic acid, after which the above solution was magnetically stirred for 30 min, and thus an  $\text{In}(\text{NO}_3)_3/\text{VO}(\text{acac})_2/\text{TBT}/\text{PVP}$  mixed solution with a Ti/In molar ratio of 4 : 1 was obtained. Then, the mixed solution was electrospun to compose the  $\text{In}(\text{NO}_3)_3/\text{VO}(\text{acac})_2/\text{TBT}/\text{PVP}$  NFs. The electrospinning parameters were set as follows: 0.4 mm for the inner diameter of the spinneret, and 20 cm and 15 kV for the distance and DC voltage between the spinneret and the collector, respectively. Finally, the obtained NFs were annealed at 550 °C for 2 h in air to remove the PVP support and crystallise the  $\text{TiO}_2/\text{InVO}_4$  NFs. A comparative sample of  $\text{TiO}_2$  NFs was also synthesized by the same electrospinning method with a solution of 0.68 g tetrabutyl titanate (TBT) and 0.14 g polyvinylpyrrolidone (PVP) in a mixed solution of 1.0 ml ethanol and 0.8 ml acetic acid.

### 2.2 Photochemical experiments

The visible-light photocatalytic activity of the nanofibers was measured from the degradation of Rhodamine B (RhB)

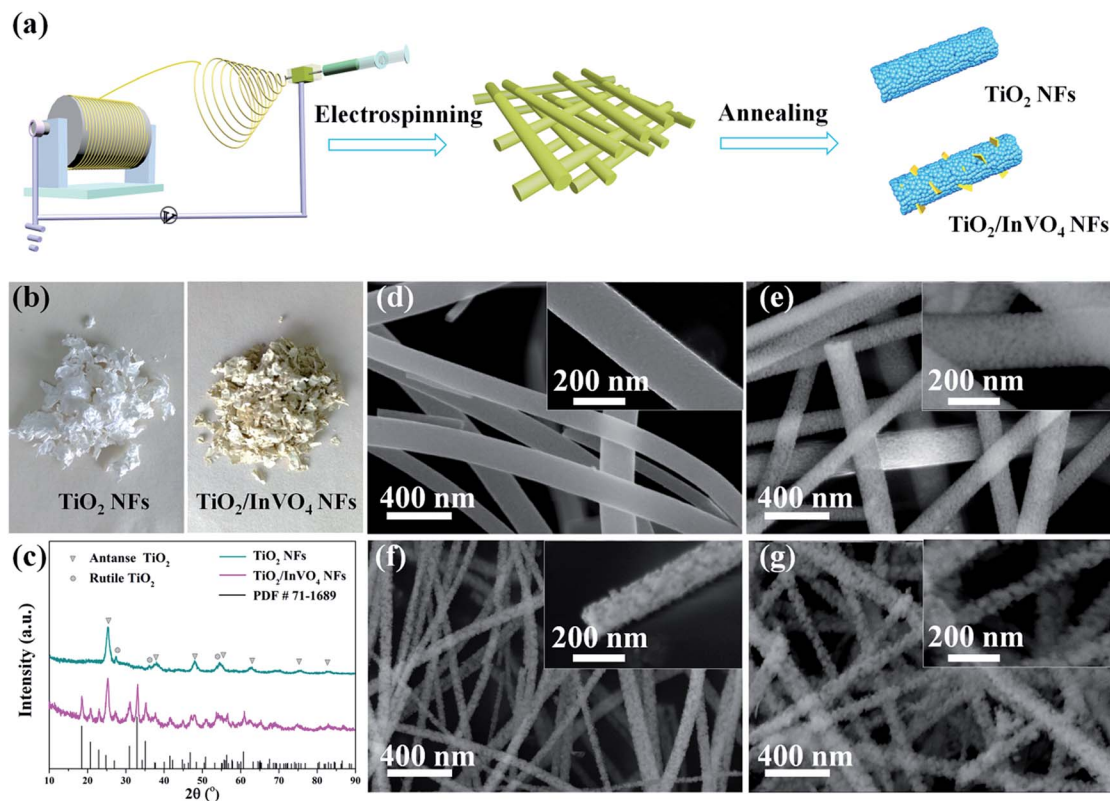


Fig. 1 (a) Schematic illustration of the fabrication process for the  $\text{TiO}_2$  NFs and  $\text{TiO}_2/\text{InVO}_4$  NFs. (b) Physical pictures and (c) XRD patterns of the  $\text{TiO}_2$  NFs and  $\text{TiO}_2/\text{InVO}_4$  NFs (Ti/In = 4 : 1). (d–g) SEM images of (d) the  $\text{TiO}_2$  NFs and (e–g)  $\text{TiO}_2/\text{InVO}_4$  NFs with Ti/In molar ratios of 8 : 1, 4 : 1, 2 : 1, respectively.



molecules. Firstly, 50 mg catalysts were added to 30 ml RhB ( $10 \text{ mg l}^{-1}$ ) solution and the suspensions were placed in dark environment for 30 min to reach an equilibrium of absorption and desorption. Secondly, a Xe lamp ( $\lambda > 420 \text{ nm}$ ) was employed for visible-light photocatalytic irradiation. At time intervals of 10 min, 3 ml suspensions were sucked and filtered to separate the catalysts. The variations in the filtrates were assessed using the change in the absorption band maximum recorded using a TU-1901 spectrophotometer.

### 2.3 Characterization

X-ray diffraction (XRD, X'pert Pro,  $\text{CuK}\alpha$ ,  $\lambda = 1.5406$ ) and high-resolution transmission electron microscopy (HRTEM, Libra 200FE) were utilized to characterize the crystal structure of the nanofibers. Energy dispersive spectroscopy (EDS) and X-ray photoelectron spectroscopy (XPS) were employed to characterize the components of the samples. The morphologies of the nanofibers were obtained by Field emission scanning electron microscopy (FESEM, Hitachi S-4800) and TEM. Nitrogen adsorption-desorption isotherms (JW-BK122 W nitrogen adsorption apparatus) were used to evaluate the Brunauer-Emmett-Teller (BET) specific surface areas of the nanofibers. Furthermore, UV-Vis absorption spectra were obtained using a UV-3150 spectrophotometer, and photoluminescence (PL) spectra were obtained using a Raman spectrometer with a 532 nm laser excitation source. Transient PL curves for the nanofibers were recorded using a FLS920 fluorescence lifetime spectrophotometer (Edinburgh Instruments, UK) with the excitation wavelength at 532 nm.

## 3. Results and discussion

$\text{TiO}_2/\text{InVO}_4$  NFs were synthesized by a one-pot electrospinning process, as shown in Fig. 1(a). Physical pictures of the samples are displayed in Fig. 1(b). It is quite distinct that the color of the  $\text{TiO}_2$  NFs is white, while the  $\text{TiO}_2/\text{InVO}_4$  NFs appear to be faint yellow. Furthermore, XRD patterns are employed to characterize the phase composition of the resulting  $\text{TiO}_2/\text{InVO}_4$  NFs, with the  $\text{TiO}_2$  NFs as a reference sample, as presented in Fig. 1(c). The diffraction peaks of the  $\text{TiO}_2$  NFs can be indexed to anatase  $\text{TiO}_2$  (PDF #21-1272) and rutile  $\text{TiO}_2$  (PDF #21-1276). In the case of the  $\text{TiO}_2/\text{InVO}_4$  NFs, a superimposed XRD pattern of  $\text{TiO}_2$  and orthorhombic  $\text{InVO}_4$  (PDF #71-1689) is observed, which demonstrates both  $\text{TiO}_2$  and  $\text{InVO}_4$  with good crystallization in the  $\text{TiO}_2/\text{InVO}_4$  NFs.

The general morphologies of the nanofibers are obtained from SEM images and the results are demonstrated in Fig. 1(d), in which it is clearly revealed that one-dimensional  $\text{TiO}_2$  and  $\text{TiO}_2/\text{InVO}_4$  structures have been successfully constructed. As shown in Fig. 1(d), the  $\text{TiO}_2$  NFs have rough and uniform morphologies, with average diameters of about 150 nm and lengths of about a few micrometers. The morphologies of the  $\text{TiO}_2/\text{InVO}_4$  NFs with different Ti/In molar ratios are presented in Fig. 1(e–g), which all have an average length of a few micrometers, as well as loose and rough surfaces. Furthermore, with a decrease in the Ti/In molar ratio, it is obvious that the

average diameter of the  $\text{TiO}_2/\text{InVO}_4$  NFs decreases and the surface of the  $\text{TiO}_2/\text{InVO}_4$  NFs becomes much more loose and rough, which can be attributed to the adjustment of the PVP amount and the epitaxial growth of  $\text{InVO}_4$  in the electrospinning process.

To further confirm the microscopic morphologies and crystal structures of the  $\text{TiO}_2/\text{InVO}_4$  NFs, TEM images are recorded in Fig. 2. It is obvious that the  $\text{TiO}_2/\text{InVO}_4$  NFs with a diameter of  $\sim 100 \text{ nm}$  (Fig. 2(a)) are composed of many distinct crystal particles and flakes, as displayed in Fig. 2(b). Then, we obtained an HRTEM image of the  $\text{TiO}_2/\text{InVO}_4$  NFs to further observe the distributional crystal particles, and the result is presented in Fig. 2(c). The lattice distance of 0.35 nm is attributed to the (101) lattice distance of anatase  $\text{TiO}_2$ , and the measured lattice fringes of 0.28 nm and 0.36 nm correspond to the interplanar spacings of the (200) and (021) planes of orthorhombic  $\text{InVO}_4$ , respectively, indicating that the  $\text{TiO}_2/\text{InVO}_4$  nanoheterostructures have been prepared successfully. Additionally, the results of the STEM-EDS elemental mapping analysis are displayed in Fig. 2(d–g) to further explore the element distributions in the  $\text{TiO}_2/\text{InVO}_4$  nanofibers. It is obvious that the  $\text{TiO}_2/\text{InVO}_4$  nanofibers are mainly composed of the metals Ti, In, and V, and the diameters of In and V are larger than that of Ti, which indicates that the flake-structure on the surfaces of the  $\text{TiO}_2/\text{InVO}_4$  NFs can be assigned to the secondary growth of  $\text{InVO}_4$ .

In order to further determine the molar ratio of elements in all the  $\text{TiO}_2/\text{InVO}_4$  NFs (Ti/In = 4 : 1), energy dispersive spectroscopic (EDS) analysis was applied and the results are shown in Fig. 3, in which it can be observed that Ti, In, V, and O appear in the  $\text{TiO}_2/\text{InVO}_4$  NFs, and the atomic ratios of Ti, In, and V are

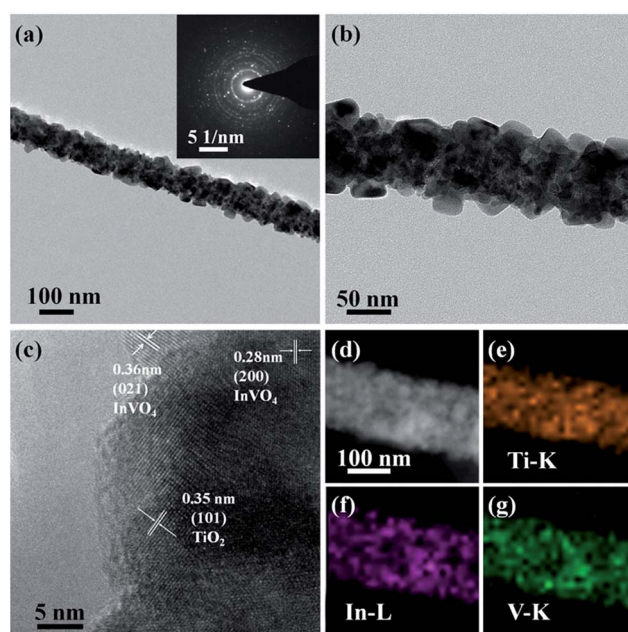


Fig. 2 (a and b) TEM images and (c) a high magnification TEM (HRTEM) image of the  $\text{TiO}_2/\text{InVO}_4$  NFs (Ti/In = 4 : 1); (d–g) STEM image of the  $\text{TiO}_2/\text{InVO}_4$  NFs (Ti/In = 4 : 1) (d), and the corresponding EDX elemental maps of Ti (e), In (f), and V (g), respectively.





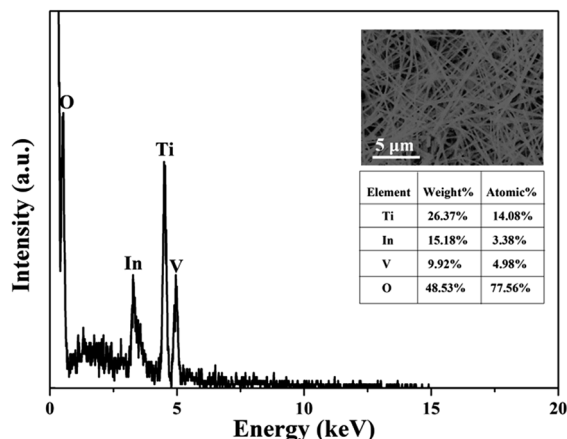


Fig. 3 EDS pattern of the  $\text{TiO}_2/\text{InVO}_4$  NFs (Ti/In = 4 : 1).

14.08%, 3.38%, and 4.98%, respectively, implying the molar ratio of Ti/In is about 4.2, which is in agreement with the set value of the Ti/In molar ratio in the electrospinning process. Furthermore, XPS measurements were employed and the results are displayed in Fig. 4. Fig. 4(a) shows the holistic survey spectrum of the  $\text{TiO}_2/\text{InVO}_4$  NFs, in which Ti, In, V, and O are detected. In addition, the Ti 2p, In 3d, and V 2p core-level spectra of the  $\text{TiO}_2/\text{InVO}_4$  NFs are shown in Fig. 4(b–d). The peaks at 444.5 eV and 452.0 eV in the In 3d core-level spectrum, as shown in Fig. 3(b), correspond to In 3d<sub>3/2</sub> and In 3d<sub>5/2</sub> for  $\text{In}^{3+}$  species, respectively.<sup>31</sup> As shown in Fig. 4(c), the V 2p peaks are located at 517.1 eV and 524.6 eV, which can be ascribed to  $\text{V}^{5+}$ .<sup>32</sup> From the Ti 2p core-level spectrum in Fig. 4(d), two clearly evident peaks centered at 463.8 and 458.2 eV can be assigned to Ti 2p<sub>1/2</sub> and Ti 2p<sub>3/2</sub>, respectively, which belong to the  $\text{Ti}^{4+}$  elemental chemical state of  $\text{TiO}_2$ .<sup>33</sup> It can be therefore concluded that the  $\text{TiO}_2/\text{InVO}_4$  NFs have been fabricated successfully.

We then investigated the photocatalytic performance of  $\text{TiO}_2$  NFs and  $\text{TiO}_2/\text{InVO}_4$  NFs with different Ti/In molar ratios

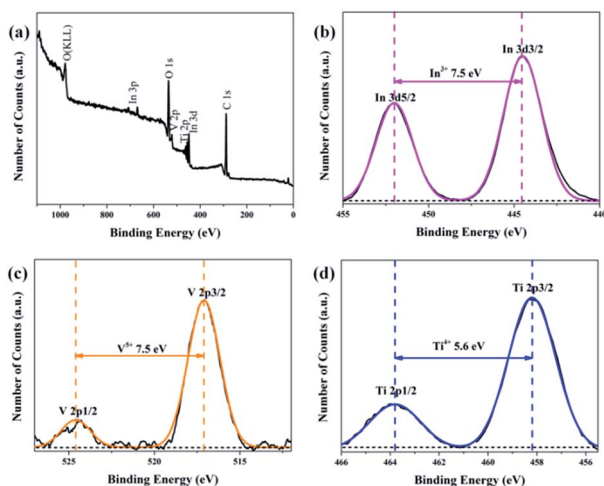


Fig. 4 (a) XPS survey spectrum of the  $\text{TiO}_2/\text{InVO}_4$  NFs (Ti/In = 4 : 1), and (b–d) high resolution XPS spectra of the In 3d, V 2p, and Ti 2p core-level binding energies, respectively.

toward the photodegradation process of RhB solution. As shown in Fig. 5(a), after adding 50 mg  $\text{TiO}_2/\text{InVO}_4$  NFs (Ti/In = 4 : 1) as a photocatalyst into RhB solution, the  $\lambda_{\text{max}}$  intensity of the absorption spectral changes of the RhB solution is significantly decreased with irradiation time. Fig. 5(b) presents the corresponding concentration change in the RhB solution when using different samples as photocatalysts under visible-light irradiation. It is obviously that after 80 min of visible-light irradiation, only 18% and 32% of RhB molecules are decomposed by the  $\text{TiO}_2$  NFs and standard P25, respectively, which can be assigned to their poor visible-light absorption and short photogenerated charge lifetime. As for the  $\text{TiO}_2/\text{InVO}_4$  NFs, at least 80% of RhB molecules are effectively decomposed, indicating that the  $\text{TiO}_2/\text{InVO}_4$  NFs achieve an outstanding enhanced visible photocatalytic performance, better than that of pure  $\text{TiO}_2$  NFs. Moreover, while using the  $\text{TiO}_2/\text{InVO}_4$  NFs with a Ti/In molar ratio of 4 : 1 as photocatalysts, about 95% of RhB molecules are decomposed. In addition, as shown in Fig. 5(c), the degradation rates obtained over the  $\text{TiO}_2/\text{InVO}_4$  NFs (Ti/In = 4 : 1),  $\text{TiO}_2/\text{InVO}_4$  NFs (Ti/In = 2 : 1),  $\text{TiO}_2/\text{InVO}_4$  NFs (Ti/In = 8 : 1), P25, and  $\text{TiO}_2$  NFs are 0.03632, 0.0238, 0.01756, 0.0033, and 0.00244, respectively. Furthermore, the photocatalytic performance of  $\text{TiO}_2/\text{InVO}_4$  NFs was enhanced with the increasing amount of  $\text{InVO}_4$  and reached the best photocatalytic activity at a Ti/In molar ratio of 4 : 1. The increasing surface area with the increase in the amount of  $\text{InVO}_4$  is beneficial for the improvement of the photocatalytic activity, which is in agreement with the morphology results and dark absorption during the photocatalysis process. However, with a further increase of  $\text{InVO}_4$  amount, the epitaxial growth of  $\text{InVO}_4$  would undermine the uniformity of the nano-heterostructures and suppress the separation of the electron-hole pairs, so superabundant  $\text{InVO}_4$  is conversely unfavorable for improving photocatalytic activity. So, the  $\text{TiO}_2/\text{InVO}_4$  NFs

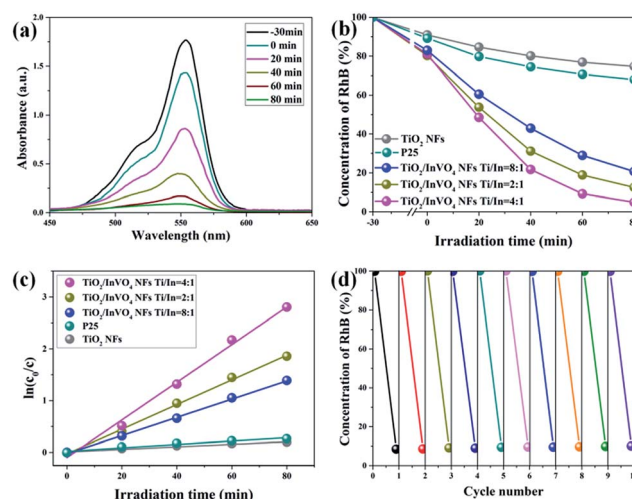


Fig. 5 (a) Absorption spectral changes of RhB solution in the presence of  $\text{TiO}_2/\text{InVO}_4$  NFs (Ti/In = 4 : 1) under visible-light irradiation. (b) Comparison of the visible-light photocatalytic degradation of RhB and (c) the photodegradation rates in the presence of  $\text{TiO}_2$  and  $\text{TiO}_2/\text{InVO}_4$  NFs. (d) Cycling tests of the photocatalytic activity of the  $\text{TiO}_2/\text{InVO}_4$  NFs (Ti/In = 4 : 1).



with a Ti/In molar ratio of 4 : 1 may exhibit outstanding synergistic effects with an appropriate surface area and nano-heterostructure, thereby allowing them to displaying the highest photocatalytic activity. Hence, we mainly conducted in-depth causal discussions on the enhanced visible-light photocatalytic performance of TiO<sub>2</sub>/InVO<sub>4</sub> NFs with a Ti/In molar ratio of 4 : 1 in the following research. Based on further practical application, the stability of the photocatalyst is a very significant factor for recycling. Herein, ten cycles of the photo-degradation behaviour of RhB are shown in Fig. 5(d) in order to evaluate the photocatalytic stability of the TiO<sub>2</sub>/InVO<sub>4</sub> NFs. After each cycle of the photocatalysis reaction process, it can be seen that there is only negligible reduction in the photocatalytic activity, indicating the excellent reusability and stability of the TiO<sub>2</sub>/InVO<sub>4</sub> NFs. In a word, TiO<sub>2</sub>/InVO<sub>4</sub> NFs exert an outstanding stability, and a much enhanced visible-light photocatalytic activity compared with pure TiO<sub>2</sub> NFs.

Based on the excellent results, we have mainly conducted in-depth causal discussions on three aspects of the enhanced visible-light photocatalytic performance of the TiO<sub>2</sub>/InVO<sub>4</sub> NFs. Firstly, it is well known that surface area is an important factor for photocatalysis.<sup>34</sup> Hence, as shown in Fig. 6(a), we employed a BET adsorption/desorption of nitrogen gas method to evaluate the specific surface area of the TiO<sub>2</sub> NFs and TiO<sub>2</sub>/InVO<sub>4</sub> NFs. The BET surface area of the TiO<sub>2</sub>/InVO<sub>4</sub> NFs, calculated from the nitrogen isotherm curve, is 30.5 m<sup>2</sup> g<sup>-1</sup>, which is about two times higher than that of the TiO<sub>2</sub> NFs (16.8 m<sup>2</sup> g<sup>-1</sup>). Obviously, the increased surface area of the TiO<sub>2</sub>/InVO<sub>4</sub> NFs would provide a larger available active area for the photocatalytic reaction. Accordingly, the increasing surface area of the TiO<sub>2</sub>/InVO<sub>4</sub> NFs would efficiently promote photocatalytic activity.

In particular, optical absorption characteristics have a direct influence on the photocatalytic activity of semiconductors. Herein, we employed UV-Vis absorbance spectroscopy to attest whether TiO<sub>2</sub>/InVO<sub>4</sub> NFs have a wider light absorption range for visible light compared with TiO<sub>2</sub> NFs, and the results are shown in Fig. 6(b). TiO<sub>2</sub> NFs present an evident absorption edge located at 400 nm, derived from the intrinsic energy gap of TiO<sub>2</sub>. The UV-Vis spectra of the TiO<sub>2</sub>/InVO<sub>4</sub> NFs reveal a wide visible-light absorption band around 400–650 nm, which contributed to the introduction of the narrow band gap InVO<sub>4</sub> semiconductor. This effectual change of the absorption spectra indicates that the TiO<sub>2</sub>/InVO<sub>4</sub> NFs have broader spectral harvesting, ultimately leading to the improvement of the visible-light photocatalytic activity.

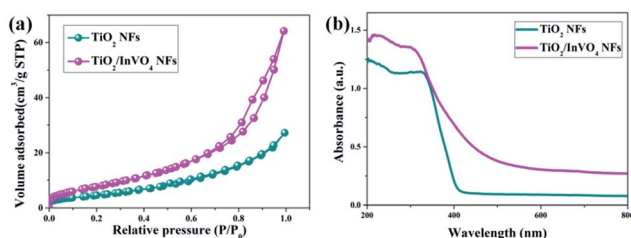


Fig. 6 (a) N<sub>2</sub> adsorption-desorption isotherms and (b) UV-Vis absorbance spectra of the TiO<sub>2</sub> NFs and TiO<sub>2</sub>/InVO<sub>4</sub> NFs.

It is fairly well acknowledged that a lower PL emission intensity of the samples under the same laser irradiation implies less electron-hole recombination.<sup>35</sup> Herein, we employed steady-state and time-resolved transient PL spectroscopy to characterize the capability of electron-hole pair separation in the nanofibers. As shown in Fig. 7(a), in the TiO<sub>2</sub> NF PL spectrum, the strong emission band at around 550–850 nm is mainly attributed to deep and shallow trap centers of oxygen defects and excitons.<sup>36</sup> However, the TiO<sub>2</sub>/InVO<sub>4</sub> NFs have a substantially lower PL intensity than the TiO<sub>2</sub> NFs, which implies that recombination of the photo-generated electron-hole pairs in the TiO<sub>2</sub>/InVO<sub>4</sub> NFs is effectively suppressed.

Time-resolved photoluminescence (TRPL) is an effective method employed to extract the carrier lifetime ( $\tau$ ), which can directly indicate various radiative and non-radiative loss channels responsible for photogenerated carrier recombination.<sup>37</sup> To further verify the nanoheterojunction's functions of electron-hole separation and carrier transfer in the TiO<sub>2</sub>/InVO<sub>4</sub> NFs, TRPL was employed at room temperature to explore the dynamics of the photogenerated charge. The transient emission spectra for the TiO<sub>2</sub> NFs and TiO<sub>2</sub>/InVO<sub>4</sub> NFs are shown in Fig. 7(b and c). The PL decay profile is fitted using a multi-exponential function as follows:<sup>38,39</sup>

$$I_t = \sum_{i=1}^n A_i \exp(-t/\tau_i) \quad (1)$$

where  $I_t$  is intensity,  $A_i$  is the relative magnitude of the  $i$ th decay, and  $\tau_i$  is the  $i$ th decay time. It can be deduced that the TiO<sub>2</sub>/InVO<sub>4</sub> NFs yield the longest decay time ( $\tau_1 = 2.047$  ns,  $A_1 = 0.1475$ ;  $\tau_2 = 27.862$  ns,  $A_2 = 0.0368$ ) compared with the TiO<sub>2</sub> NFs ( $\tau_1 = 1.339$  ns,  $A_1 = 0.2172$ ;  $\tau_2 = 23.686$  ns,  $A_2 = 0.212$ ). Furthermore, the fast factor ( $\tau_1$ ) commonly corresponds to the non-radiative relaxation process, owing to oxide defects,<sup>40</sup> and the slow factor ( $\tau_2$ ) is attributed to the radiative pathway, related to the recombination of photogenerated electron-hole pairs.<sup>41</sup> Furthermore, the average lifetimes ( $\tau_{ave}$ ) can be deduced through the following equation for a general comparison of the carrier lifetime:<sup>42</sup>

$$\tau_{ave} = f_1 \tau_1 + f_2 \tau_2 = \frac{A_1 \tau_1^2 + A_2 \tau_2^2}{A_1 \tau_1 + A_2 \tau_2} \quad (2)$$

The values for the average time calculated based on two-exponential decays for the TiO<sub>2</sub>/InVO<sub>4</sub> NFs and TiO<sub>2</sub> NFs are 22 ns and 15 ns, respectively. In order to compare the separation efficiency of the TiO<sub>2</sub>/InVO<sub>4</sub> heterostructures, we list the carrier lifetimes of different TiO<sub>2</sub>-based heterostructures reported previously in Table 1, and it is obvious that the TiO<sub>2</sub>/InVO<sub>4</sub> NFs with tailored heterostructure features exhibit longer carrier lifetimes than TiO<sub>2</sub>/SiO<sub>2</sub>, TiO<sub>2</sub>/In<sub>2</sub>S<sub>3</sub>, and TiO<sub>2</sub>/MoS<sub>2</sub>, implying that this kind of heterostructure prepared by electrospinning can provide ample heterojunction interfaces for more separation channels for photogenerated electron-hole pairs.

To better understand the charge separation in TiO<sub>2</sub>/InVO<sub>4</sub> NFs, a schematic illustration of the efficient separation and



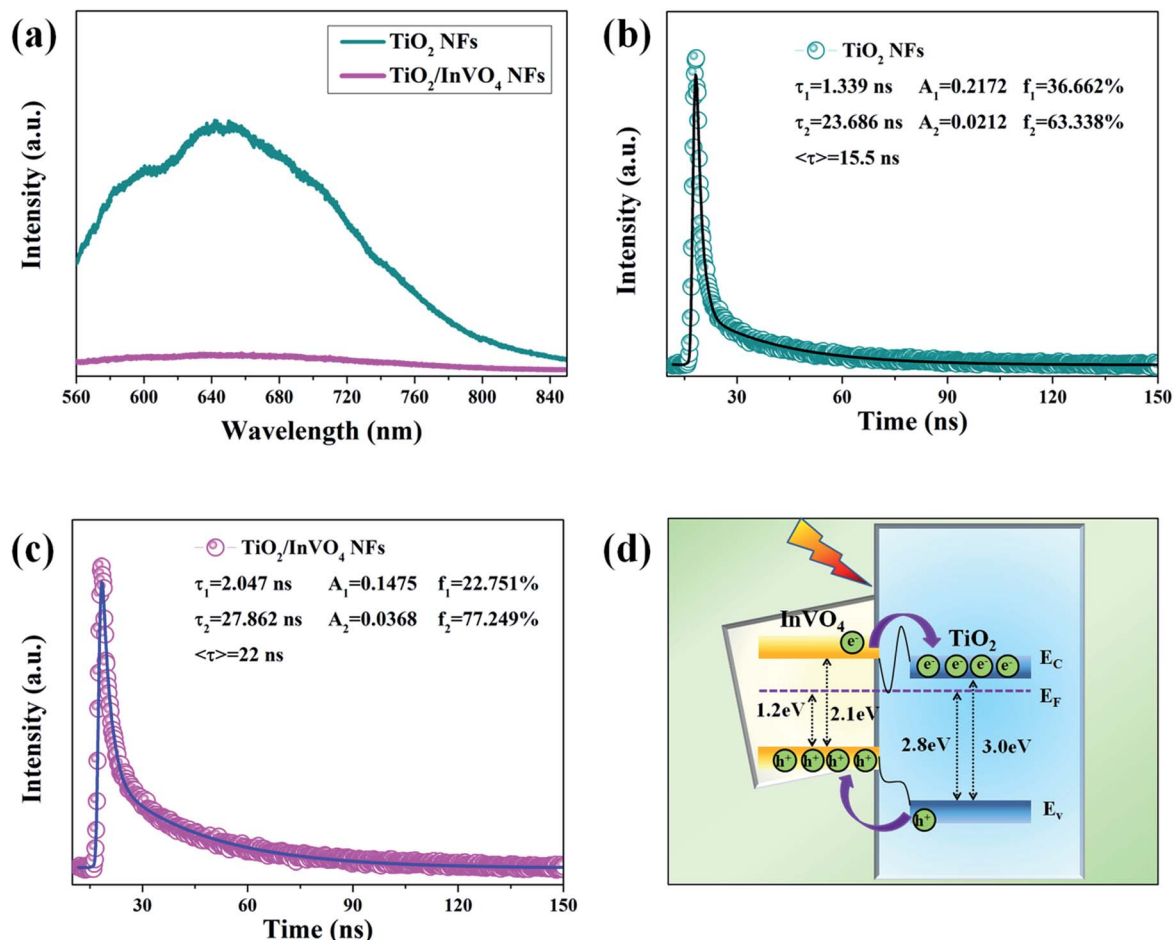


Fig. 7 (a) Steady-state PL spectra of TiO<sub>2</sub> NFs and TiO<sub>2</sub>/InVO<sub>4</sub> NFs (Ti/In = 4 : 1). (b and c) Time-resolved transient PL decay of TiO<sub>2</sub> NFs and TiO<sub>2</sub>/InVO<sub>4</sub> NFs (Ti/In = 4 : 1), respectively. (d) Schematic illustration of energy band matching and the proposed mechanism of charge carrier transition for TiO<sub>2</sub>/InVO<sub>4</sub> nanoheterojunctions under visible-light irradiation, including conduction bands ( $E_C$ ), valence bands ( $E_V$ ), and Fermi levels ( $E_F$ ).

transport of photogenerated charge in the TiO<sub>2</sub>/InVO<sub>4</sub> NFs is represented in Fig. 7(d). The standard literature energy levels of TiO<sub>2</sub> and InVO<sub>4</sub> (conduction bands of  $-4.0$  eV and  $-3.6$  eV, valence bands of  $-7.0$  eV and  $-5.7$  eV, and Fermi levels of  $-4.2$  eV and  $-4.5$  eV, vs. the vacuum level, respectively) were employed for the energy band matching analysis here.<sup>45</sup> The matching energy band between InVO<sub>4</sub> and TiO<sub>2</sub> is shown in Fig. 6(d), when the nanoheterostructures are formed, the Fermi energy bands of TiO<sub>2</sub> and InVO<sub>4</sub> are at the same level, which thus leads both the conduction band ( $E_C$ ) and valence band ( $E_V$ ) of InVO<sub>4</sub> to locate above those of TiO<sub>2</sub>. Under visible-light irradiation, InVO<sub>4</sub> in the TiO<sub>2</sub>/InVO<sub>4</sub> NFs is photoexcited to

produce electron-hole pairs, and owing to the incomparable nanoheterojunction structure formed at the interfaces of TiO<sub>2</sub> and InVO<sub>4</sub>, the photogenerated electrons can facilitate transport to the  $E_C$  of TiO<sub>2</sub>. Hereby, numerous photogenerated electrons transport from the  $E_C$  of InVO<sub>4</sub> to that of TiO<sub>2</sub>, and photogenerated holes concentrate on the  $E_V$  of InVO<sub>4</sub>. In this way, the separation of the photogenerated charge can be efficiently facilitated, thereby prolonging the carrier lifetimes and resulting in the enhanced photocatalytic activity of the TiO<sub>2</sub>/InVO<sub>4</sub> NFs under visible-light irradiation.

## 4. Conclusions

In summary, TiO<sub>2</sub>/InVO<sub>4</sub> NFs were successfully fabricated by a facile one-pot electrospinning method. The TiO<sub>2</sub>/InVO<sub>4</sub> NFs showed a significantly enhanced photocatalytic performance; almost 95% of RhB molecules were decomposed within 80 min by the TiO<sub>2</sub>/InVO<sub>4</sub> NFs (Ti/In = 4 : 1), but only 18% of RhB molecules were decomposed by pure TiO<sub>2</sub> NFs. Moreover, the time-resolved transient PL spectra reveal that the TiO<sub>2</sub>/InVO<sub>4</sub> NFs exhibit a prolonged average carrier lifetime of 22 ns, more

Table 1 Carrier lifetimes of different TiO<sub>2</sub>-based heterostructures

Heterostructure composites	TiO <sub>2</sub> /InVO <sub>4</sub> NFs	TiO <sub>2</sub> /SiO <sub>2</sub> film <sup>43</sup>	TiO <sub>2</sub> /In <sub>2</sub> S <sub>3</sub> nanobelts <sup>40</sup>	TiO <sub>2</sub> /MoS <sub>2</sub> nanocomposite <sup>44</sup>
$\tau_1$ (ns)	2.047	0.0824	0.67	—
$\tau_2$ (ns)	27.862	0.898	4.64	—
$T_{ave}$ (ns)	22	—	—	9.49



than that of the TiO<sub>2</sub> NFs, which can promote photogenerated carrier separation. Accordingly, the resulting TiO<sub>2</sub>/InVO<sub>4</sub> NFs display excellent visible-light photocatalytic performance, owing to their prominent visible-light harvesting and electron-hole separation properties. It is indisputable that TiO<sub>2</sub>/InVO<sub>4</sub> NFs may shed new light on highly efficient visible-light nano-heterostructured photocatalysts with longer carrier lifetimes.

## Conflicts of interest

There are no conflicts to declare.

## Acknowledgements

This work was supported by the National Natural Science Foundation of China (No. 11704354) and the Hunan Provincial Innovation Foundation for Postgraduate (No. 8443|431000203431000203).

## Notes and references

- 1 D. M. Schultz and T. P. Yoon, *Science*, 2014, **343**, 1239176.
- 2 K. Nakata, B. Liu, Y. Goto, T. Ochiai, M. Sakai, H. Sakai, T. Murakami, M. Abe and A. Fujishima, *Chem. Lett.*, 2011, **40**, 1161–1162.
- 3 J. Ran, J. Zhang, J. Yu, M. Jaroniec and S. Z. Qiao, *Chem. Soc. Rev.*, 2014, **43**, 7787–7812.
- 4 A. Fujishima and K. Honda, *Nature*, 1972, **238**, 37.
- 5 Y. Bai, I. Mora-Sero, F. D. Angelis, J. Bisquert and P. Wang, *Chem. Rev.*, 2014, **114**, 10095–10130.
- 6 S. G. Kumar and L. G. Devi, *J. Phys. Chem. A*, 2011, **115**, 13211–13241.
- 7 C. P. Sajan, S. Wageh, A. A. Al-Ghamdi, J. Yu and S. Cao, *Nano Res.*, 2016, **9**, 3–27.
- 8 J. Hensel, G. Wang, Y. Li and J. Z. Zhang, *Nano Lett.*, 2010, **10**, 478–483.
- 9 R. Asahi, T. Morikawa, T. Ohwaki, K. Aoki and Y. Taga, *Science*, 2001, **293**, 269–271.
- 10 T. Huang, S. Mao, J. Yu, Z. Wen, G. Lu and J. Chen, *RSC Adv.*, 2013, **3**, 16657–16664.
- 11 W. He, Z. Fang, K. Zhang, X. Li, D. Ji, X. Jiang, C. Qiu and K. Guo, *RSC Adv.*, 2015, **5**, 54853–54860.
- 12 X. Chen, L. Liu, Y. Y. Peter and S. S. Mao, *Science*, 2011, **331**, 746–750.
- 13 Y. Shi, D. Yang, Y. Li, J. Qu and Z. Z. Yu, *Appl. Surf. Sci.*, 2017, **426**, 622–629.
- 14 X. Zhang, Z. Shen, C. Cheng, L. Shi, R. Cheng and J. Dong, *RSC Adv.*, 2017, **7**, 52172–52179.
- 15 C. Cheng, J. Shi, Y. Hu and L. Guo, *Nanotechnology*, 2017, **28**, 164002.
- 16 H. Zhang, F. Liu, H. Wu, X. Cao, J. Sun and W. Lei, *RSC Adv.*, 2017, **7**, 40327–40333.
- 17 M. N. Ha, F. Zhu, Z. Liu, L. Wang, L. Liu, G. Lu and Z. Zhao, *RSC Adv.*, 2016, **6**, 21111–21118.
- 18 H. Wang, L. Zhang, Z. Chen, J. Hu, S. Li, Z. Wang, J. Liu and X. Wang, *Chem. Soc. Rev.*, 2014, **43**, 5234–5244.
- 19 C. Cheng, W. Ren and H. Zhang, *Nano Energy*, 2014, **5**, 132–138.
- 20 P. G. Ramos, E. Flores, L. A. Sánchez, R. J. Candal, M. Hojamberdiev, W. Estrada and J. Rodriguez, *Appl. Surf. Sci.*, 2017, **426**, 844–851.
- 21 F. Tian, D. Hou, F. Hu, K. Xie, X. Qiao and D. Li, *Appl. Surf. Sci.*, 2017, **391**(Part B), 295–302.
- 22 X. Ren, X. Qi, Y. Shen, S. Xiao, G. Xu, Z. Zhang, Z. Huang and J. Zhong, *J. Phys. D: Appl. Phys.*, 2016, **49**, 315304.
- 23 S. P. Adhikari, G. P. Awasthi, J. Lee, C. H. Park and C. S. Kim, *RSC Adv.*, 2016, **6**, 55079–55091.
- 24 F. Xu, J. Zhang, B. Zhu, J. Yu and J. Xu, *Appl. Catal., B*, 2018, **230**, 194–202.
- 25 X. Zhang, *Catal. Lett.*, 2014, **144**, 1253–1257.
- 26 Y. Yan, X. Liu, W. Fan, P. Lv and W. Shi, *Chem. Eng. J.*, 2012, **200–202**, 310–316.
- 27 J. Shen, H. Yang, Y. Feng, Q. Cai and Q. Shen, *Solid State Sci.*, 2014, **32**, 8–12.
- 28 I. A. Perales-Martínez, V. Rodríguez-González, S. W. Lee and S. Obregón, *J. Photochem. Photobiol., A*, 2015, **299**, 152–158.
- 29 Y. Min, K. Zhang, Y. C. Chen and Y. G. Zhang, *Ultrason. Sonochem.*, 2012, **19**, 883–889.
- 30 L. Ge, M. Xu and H. Fang, *Mater. Lett.*, 2007, **61**, 63–66.
- 31 F. Guo, W. Shi, X. Lin, X. Yan, Y. Guo and G. Che, *Sep. Purif. Technol.*, 2015, **141**, 246–255.
- 32 A. Chakrabarti, K. Hermann, R. Druzinic, M. Witko, F. Wagner and M. Petersen, *Phys. Rev. B: Condens. Matter Mater. Phys.*, 1999, **59**, 10583–10590.
- 33 H. Li, Y. Wang, G. Chen, Y. Sang, H. Jiang, J. He, X. Li and H. Liu, *Nanoscale*, 2016, **8**, 6101–6109.
- 34 G. Tian, Y. Chen, W. Zhou, K. Pan, C. Tian, X. Huang and H. Fu, *CrystEngComm*, 2011, **13**, 2994.
- 35 Z. Zhang, C. Shao, X. Li, L. Zhang, H. Xue, C. Wang and Y. Liu, *J. Phys. Chem. C*, 2010, **114**, 7920–7925.
- 36 K. Iijima, M. Goto, S. Enomoto, H. Kunugita, K. Ema, M. Tsukamoto, N. Ichikawa and H. Sakama, *J. Lumin.*, 2008, **128**, 911–913.
- 37 H. H. Wang, Q. Chen, H. Zhou, L. Song, Z. S. Louis, N. D. Marco, Y. Fang, P. Sun, T. B. Song, H. Chen and Y. Yang, *J. Mater. Chem. A*, 2015, **3**, 9108–9115.
- 38 J. L. Wu, F. C. Chen, Y. S. Hsiao, F. C. Chien, P. L. Chen, C. H. Kuo, M. H. Huang and C. S. Hsu, *ACS Nano*, 2011, **5**, 959–967.
- 39 S. W. Cao, X. F. Liu, Y. P. Yuan, Z. Y. Zhang, Y. S. Liao, J. Fang, S. C. J. Loo, T. C. Sum and C. Xue, *Appl. Catal., B*, 2014, **147**, 940–946.
- 40 Y. Li, T. Li, J. Tian, X. Wang and H. Cui, *Part. Part. Syst. Charact.*, 2017, **34**, 1700127.
- 41 X. Zeng and W. Qin, *Mater. Lett.*, 2016, **182**, 347.
- 42 B. R. Masters, *J. Biomed. Opt.*, 2008, **13**, 029901.
- 43 K. Miyashita, S. Kuroda, S. Tajima, K. Takehira, S. Tobita and H. Kubota, *Chem. Phys. Lett.*, 2003, **369**, 225–231.
- 44 H. S. Han, K. M. Kim, C. W. Lee, C. S. Lee, R. C. Pawar, J. L. Jones, Y. R. Hong, J. H. Ryu, T. Song, S. H. Kang, H. Choi and S. Mhin, *Phys. Chem. Chem. Phys.*, 2017, **19**, 28207–28215.
- 45 G. Xiao, X. Wang, D. Li and X. Fu, *J. Photochem. Photobiol., A*, 2008, **193**, 213–221.

